HHS Public Access

Author manuscript

J Biomed Mater Res B Appl Biomater. Author manuscript; available in PMC 2017 November 01.

Published in final edited form as:

J Biomed Mater Res B Appl Biomater. 2016 November ; 104(8): 1679–1690. doi:10.1002/jbm.b.33515.

Injected Biodegradable Polyurethane Scaffolds Support Tissue Infiltration and Delay Wound Contraction in a Porcine Excisional Model

Elizabeth J. Adolph, Ph.D.[*,1], **Ruijing Guo**[*,1], **Alonda C. Pollins, M.L.I.**[2], **Katarzyna Zienkiewicz**[1], **Nancy Cardwell, B.S.**[2], **Jeffrey M. Davidson, Ph.D.**[3,4], **Scott A. Guelcher, Ph.D.**[1,5,6], and **Lillian B. Nanney, Ph.D.**[2,7]

[1]Department of Chemical and Biomolecular Engineering, Vanderbilt University, Nashville, TN

[2]Department of Plastic Surgery, Vanderbilt University Medical Center, Nashville, TN

[3]Research Service, VA Tennessee Valley Healthcare System, Nashville, TN

[4]Department of Pathology, Microbiology and Immunology, Vanderbilt University Medical Center, Nashville, TN

[5]Department of Biomedical Engineering, Vanderbilt University, Nashville, TN

[6]Center for Bone Biology, Vanderbilt University Medical Center, Nashville, TN

[7]Department of Cell & Developmental Biology, Vanderbilt University Medical Center, Nashville, TN

Abstract

The filling of wound cavities with new tissue is a challenge. We previously reported on the physical properties and wound healing kinetics of prefabricated, gas-blown polyurethane (PUR) scaffolds in rat and porcine excisional wounds. To address the capability of this material to fill complex wound cavities, this study examined the *in vitro* and *in vivo* reparative characteristics of injected PUR scaffolds employing a sucrose porogen. Using the porcine excisional wound model, we compared reparative outcomes to both preformed and injected scaffolds as well as untreated wounds at 9, 13, and 30 days after scaffold placement. Both injected and preformed scaffolds delayed wound contraction by 19% at 9 days and 12% at 13 days compared to non-treated wounds. This stenting effect proved transient since both formulations degraded by day 30. Both types of scaffolds significantly inhibited the undesirable alignment of collagen and fibroblasts through day 13. Injected scaffolds were highly compatible with sentinel cellular events of normal wound repair cell proliferation, apoptosis, and blood vessel density. The present study provides further evidence that either injected or preformed PUR scaffolds facilitate wound healing, support tissue infiltration and matrix production, delay wound contraction, and reduce scarring in a clinically relevant animal model, which underscores their potential utility as a void-filling platform for large cutaneous defects.

Corresponding Author: Lillian B. Nanney, 1161 21st Ave S., Nashville, TN 37212-2631, Phone: 615-322-7265, Fax: 615-343-2050, Lillian.nanney@vanderbilt.edu.

*equal contributions

Keywords

wound repair; polyurethane scaffold; porcine model; biodegradable; wound contraction

Introduction

The number of people affected by chronic wounds is growing rapidly due to the aging of the population and a rising incidence of diseases such as diabetes and obesity [1-4]. Reports estimate that $25 billion is spent annually on treatment for chronic wounds in the United States [1-3]. Furthermore, patients with either acute wounds or scars that result from surgical or traumatic injuries require healthcare that costs $12 billion annually [1]. The morbidity, incidence, and cost of these cutaneous defects create an unmet need for cost-effective wound care products that restore tissue integrity in a manner that restores the skin to its native viscoelastic properties Presently there are no therapeutics or devices that either restore skin integrity of chronic wounds within a few days to weeks or restore tissue deficits of acute wounds without hypertrophic scarring (robust fibrosis), which disrupts the functional and aesthetic properties of the skin.

Injectable and settable biomaterials, that can conform to fill deep tissue defects and can incorporate and deliver biologics at the point of care, offer volumetric and topographic customization. These materials and techniques may offer a promising approach to wound healing [5]. Successful injectable scaffolds must meet several requirements. The reactants and intermediates must be non-cytotoxic, and the reaction exotherm must be minimal [5,6]. The biomaterial must be flowable for a sufficient amount of time (i.e., working time) so that it can be applied as a liquid, and it must cure within minutes (i.e., setting time) to permit patient movement. In addition, such scaffolds must have reproducible porosity, permeability, and pore size that collectively are sufficient for cell migration, nutrient exchange, and tissue ingrowth [7].

A variety of matrix-derived scaffolds are currently available for wound repair and regeneration, such as Oasis™, Alloderm™, and Integra™. However, these materials comprise preformed thin sheets that are placed into the wound [8,9]. While injectable versions of these matrix-derived scaffolds are available, such as Integra® Flowable Wound Matrix, Cymetra® Micronized Alloderm® Tissue, and Medifil® Collagen Particles [10,11], they are not settable and therefore do not have sufficient mechanical properties to delay or minimize wound contraction by stenting the wound [12]. Crosslinkable polymers offer the advantages of *in situ* curing and tunable mechanical properties. In a rat excisional model, we recently showed that injected lysine-derived poly(ester urethane) (PUR) scaffolds with dermis-like bulk modulus were capable of stenting wounds, leading to delayed wound contraction while promoting cellular infiltration and matrix remodeling [13]. Furthermore, these PUR scaffolds have been reported to promote ingrowth of new tissue and to degrade to non-cytotoxic breakdown products in both rodent [12,14-17] and porcine [12] wound healing models. PUR scaffolds have tunable mechanical and degradation properties [18], can be injected into tissue defects [12,19,20], and are useful for local delivery of biologics [17,21,22].

We hypothesized that injectable PUR scaffolds could be formulated to stent wounds and mitigate wound contracture while creating a favorable environment for restoration of cutaneous tissue architectures. A limited number of studies have investigated cutaneous void fillers in full-thickness excisional wounds in the pig, which is a more representative model of human wound healing environment than rodents. Both pigs and humans have comparable dermal and epidermal thickness and similar density and distribution of blood vessels, sweat glands, and hair follicles [23]. Furthermore, pigs and humans heal primarily through epithelialization and granulation tissue formation while loose-skinned rodents heal mainly through wound contraction [23]. We recently reported that prefabricated PUR scaffolds showed cellular infiltration and deposition of new extracellular matrix in the porcine model [24], but the ability of injected scaffolds to set and cure *in situ* was reduced by the highly exudative nature of porcine full-thickness excisional wounds. In this study, reformulated injectable PUR scaffolds were compared to prefabricated PUR implants and untreated defects in order to evaluate their ability to support cellular infiltration and facilitate wound healing. The physical, mechanical, and rheological properties of the injected scaffolds were characterized *in vitro*. In the porcine excisional wound portion of this study, we sought to document the impact of both injected and prefabricated PUR scaffolds on our primary outcome – lessening of wound contraction through a stenting mechanism., Epithelialization, cell proliferation and apoptosis, macrophage presence, and blood vessel formation were examined as secondary outcome measures of the quality of the repair in the presence of injectable PUR scaffolds.

Methods

Materials

Glycolide and D,L-lactide were obtained from Polysciences (Warrington, PA). Glycerol was purchased from Acros Organics (Morris Plains, NJ). Lysine triisocyanate-poly(ethylene glycol) (LTI-PEG) prepolymer was obtained from Ricerca (Concord, OH). TEGOAMIN33, a tertiary amine catalyst composed of 33 wt % triethylene diamine (TEDA) in dipropylene glycol, was received from Goldschmidt (Hopewell, VA). Sucrose was obtained from Spectrum® (New Brunswick, NJ), and stannous octoate catalyst was purchased from Nusil Technology (Carpinteria, CA). All other reagents were obtained from Sigma–Aldrich (St. Louis, MO). Glycerol was dried at 10 mm Hg for 3 h at 80°C and ε-caprolactone was dried over anhydrous magnesium sulfate prior to use. All other materials were used as received.

PUR Scaffold Synthesis

Scaffolds were synthesized by two-component reactive liquid molding of LTI-PEG prepolymer with a hardener. Granular sucrose (300 – 500 μm), a water-soluble porogen, was added at 40 (P40) or 70 (P70) wt-% (Table 1) to increase permeability and limit expansion due to gas foaming. The hardener comprised 100 parts polyester triol, 5 parts per hundred parts polyol (pphp) water, and 5.5 pphp TEGOAMIN catalyst (30% solution in dipropylene glycol). The polyester triol (900 g mol^{-1}) was synthesized by reacting a glycerol starter with cyclic ester monomers (60 mol-% ε-caprolactone, 30 mol-% glycolide, and 10 mol-% D,L-lactide) in the presence of a stannous octoate catalyst[25]. After carrying out the reaction under dry argon for 48 h at 140°C, the resulting polyester triol was vacuum-dried at 80°C for

24 h. To synthesize PUR scaffolds, the hardener was combined with the sucrose particles and mixed with a spatula for 30 sec. The prepolymer (NCO:OH equivalent ratio = 1.15) was then added and mixed for another 30 sec. The reactive mixture was injected into molds for *in vitro* studies or to prepare implants for the pig study. Alternatively, the reactive PUR mixture was injected directly into full-thickness porcine excisional wounds.

Physical and Mechanical Properties

Scaffold densities and porosities were determined from mass and volume measurements of triplicate cylindrical foam cores. To determine physical properties after leaching of the sucrose particles, scaffolds (n=3) were incubated in DPBS on a shaker for 72 h. Scaffolds were then blotted dry and vacuum-dried for 24 – 48 h. The pore size distribution was assessed by scanning electron microscopy (Hitachi S-4200 SEM, Finchampstead, UK) after gold sputter coating with a Cressington Sputter Coater (Vanderbilt Institute for Nanoscale Science and Engineering).

Mechanical testing was performed using a TA Instruments Q800 Dynamic Mechanical Analyzer (DMA) in compression mode (New Castle, DE). Samples (n=3) were leached in DPBS for three days prior to mechanical testing. Stress–strain curves were generated by compressing wet cylindrical 12 × 8 mm samples at 37°C at a rate of 10% strain per min until they reached 50% strain. The bulk modulus was determined from the slope of the initial linear region of each stress–strain curve.

Permeability

The permeability of PUR scaffolds cured in different environments was investigated. The reactive mixture was injected into either empty Teflon containers (dry environment) or Teflon containers partially filled with water to create a wet environment to mimic surgery conditions and allowed to cure. Scaffolds were cut into 2 × 2 × 0.5 cm pieces. During scaffold formation, a film with lower porosity than the bulk material formed on the surface. Permeability was measured before and after removal of the surface film. To determine permeability after leaching, scaffolds were incubated in DPBS on a shaker for 72 h. Scaffolds were then dried under vacuum for 24 – 48 h. Air permeability of PUR scaffolds (n=3) was determined using the constant pressure gradient method. The air flow rate (Q) necessary to maintain a pressure gradient (ΔP ΔP) of 0.12 kPa was measured, and the permeability (k) was calculated by applying Darcy's law.

$$Q=\frac{kA}{\mu}\frac{\Delta P}{L} \quad (1)$$

where L is the scaffold thickness, A is the scaffold cross-sectional area, and Δis the dynamic viscosity of air at room temperature.

Rheological Properties

The scaffold cure profile was measured using a TA Instruments parallel plate rheometer (AR 2000ex) operating in dynamic mode with 25 mm disposable aluminum plates (New Castle, DE). After mixing the LTI-PEG with the hardener and sucrose for 30 s, the reaction mixture was loaded onto the bottom plate of the rheometer. An oscillation time sweep was run with a controlled strain of 1% and a frequency of 6.28 rad/s in order to obtain the cure profile. The storage modulus (G') and loss modulus (G'') were determined as a function of time. The working time was determined to be the G-crossover point. To measure the tack-free time, the surface of the foam was contacted with a spatula at regular one-minute intervals. The tack-free time was determined to be the amount of time until the foam no longer sticks to the spatula. Technical replicates, n=3.

Pig Surgery

All surgical procedures were reviewed and approved by the local Institutional Animal Care and Use Committee. Regulations stipulated in the NIH Guide for the Care and Use of Laboratory Animals (8^{th} Edition, 2011) and the USDA were observed. Power analysis indicated n=7 wounds per treatment group were sufficient to attain statistical confidence ($p<0.05$). The capacity of the preformed and injected scaffolds to facilitate healing in full-thickness cutaneous defects was evaluated in an excisional wound model (9 cm^2) in five female Yorkshire pigs (average weight = 25.7 ± 0.9 kg). Treatment groups included nontreated (NT) wounds (negative control), injected scaffolds + 70% sucrose (I70), injected scaffolds + 40% sucrose (I40), and preformed scaffolds + 40% sucrose (P40). Two pigs were euthanized both at 9 and 13 days, and 1 pig at 30 days after application of the scaffolds.

One 9-day and one 13-day animal were initially tested. Due to the poor initial *in vivo* performance of injected PUR scaffolds with 70% sucrose in these animals, this treatment group was discontinued in the remaining 3 animals. Therefore, the total number of wounds per treatment group for all groups except the I70 group are n=9 for 9 and 13 days, and n=5 from 1 animal for 30 days (Table 1). For the I70 treatment, n=4 for 9 and 13 days. Treatment locations were randomized at the time of application. Excisional wounds were created 24 h prior to scaffold implantation to bypass the acute, hemostatic phase of repair. Buprenex (analgesic) and cefazolin (antibiotic) were given at the time of surgery. For the remainder of the study, the analgesic fentanyl was applied in a 50 mcg/hr transdermal patch that was replaced every three days, and 500 mg of the antibiotic cephalexin was given twice daily.

Preformed scaffolds were cut into implants, sterilized using ethylene oxide, and then leached in sterile DPBS for 72 h. For injectable scaffolds containing 40% or 70% sucrose, reactants were sterilized prior to scaffold formation. Polyester triol, LTI-PEG prepolymer, and TEGOAMIN catalyst were sterilized using gamma irradiation. Sucrose was sterilized by ethylene oxide exposure. Water was sterilized by microfiltration (0.2 μm). Immediately prior to application of the injectable foams, the hardener component was added to the sucrose and mixed for 30 sec with a spatula. The prepolymer was added and mixed for 30 sec. The resulting mixture (1 g) was then spread in the wound bed with a spatula and allowed to cure. Preformed scaffolds were loosely held in place by an X-shaped configuration of spanning sutures that were anchored in intact adjacent skin. Each wound was dressed with TELFA

non-adherent dressing (Medline, Mundelein, IL) and covered with OPSITE adhesive film (Smith & Nephew, St. Petersburg, FL). The trunk of the pig was enclosed in tube gauze that was secured with Vetwrap bandaging tape (3M, St. Paul, MN). Wounds were cleaned and dressings were changed every 2-3 days.

Tissue Analysis

At the conclusion of the *in vivo* studies, wound tissues were fixed in neutral buffered formalin and embedded in paraffin. One section from each tissue was stained by Gomori's trichrome to assess matrix accumulation and the alignment of cells and collagen fibers. Reparative responses of tissues were examined and quantified using immunohistochemical markers and procedures that we have previously validated [24,26,27]. In brief, six high powered fields per tissue section were photographed and the absolute value of positive cells were counted and averaged per our standard procedure [24,26,27]. Actively proliferating cells were immunostained for Ki-67 antigen [24,26,27]. Macrophage infiltration into repairing tissues was assessed using MAC387 antisera (AbD Serotec, Raleigh, NC) [24,26,27]. Fragmented DNA of apoptotic cells was visualized with the DeadEnd Colorimetric TUNEL System (Promega Corporation, Madison, WI) [24,26,27]. The density of new capillaries in the wound bed was determined by immunostaining using antisera for von Willebrand Factor (VWF) [24,26,27].

Local Fiber Alignment Analysis

Collagen fiber analysis was conducted from tissue sections stained with Gomori's trichrome with green dye. The fiber alignment evaluation was carried out with Image J plug-in "Orientation J"[28,29] and was based on n=3 wounds for each experimental group. Collagen fiber directional variance within selected regions of interest (ROI) in wound tissues was calculated from the local angle distribution by analyzing low magnification (2×) images at each pixel using coherency-weighted alignment. To compare the local fiber alignment, directional variance was computed and normalized to the total pixels of the selected ROI. To visualize local orientation properties of collagen fibers in the wounds, high magnification (20×) images were utilized and the structure tensor for each 5-pixel unit was computed. The generated images were shown in HSB mode: hue indicated local orientation and saturation indicated local coherency.

Statistical Analysis

Two-way analysis of variance (ANOVA) was also used to evaluate wound contraction (the primary outcome) against all treatment groups and time points. One-way ANOVA was used to evaluate the statistical significance of the results among the treatment groups at each individual time point. Individual t-tests were performed for post-hoc analysis between treatments. All p-values ≤ 0.05 were considered statistically significant. Data are expressed as mean ± standard error unless otherwise indicated.

Results

Physical, Mechanical, and Rheological Properties of PUR Scaffolds

Scaffold density, porosity, and pore size were measured before and after sucrose leaching (Table 2). As expected, leaching significantly decreased the density and increased the

porosity of the P40 and P70 scaffolds. The bulk modulus decreased after leaching, but this difference was only significant for P70 scaffolds. SEM imaging was performed to analyze pore morphology and sucrose bead distribution (Figure 1). SEM images show sucrose beads embedded in the scaffold walls prior to leaching (Figures 1A and B). After leaching, sucrose particles were no longer visible (Figures 1C and D). Figure 2A shows the changes in rheological properties of P40 scaffolds during polymerization. The working time was identified as the gel point, which was determined from the G′ (elastic component)-G″ (viscous component) crossover point (dashed line). The working time of P40 scaffolds was 4.8 ± 1.2 min. The tack-free time, determined as the time at which the scaffold no longer stuck to a metal spatula, was 16 ± 3 min (Figure 2B).

Permeability of PUR Scaffolds

The permeability of PUR scaffolds was evaluated using the constant pressure gradient method (Table 3). Four parameters were varied: sucrose loading (40 or 70 wt-%), foaming environment (wet or dry), leaching of the sucrose beads, and the presence or absence of a surface film. Some scaffolds were foamed in a wet environment to mimic the conditions of injection in the porcine excisional wound study, in which the wound bed is moderately exudative in the early acute period. Since the surface of PUR scaffolds has a lower porosity than the bulk material, the surface film of some scaffolds was removed. Increasing the sucrose from 40% to 70%, leaching the scaffolds, foaming the scaffolds in a wet environment, and removing the surface film were all factors that increased the permeability of the scaffolds.

Wound Characteristics

Representative images of porcine excisional wound tissue sections stained with trichrome from each of the 3 time points (Days 9, 13, and 30) are shown in Figure 3. By day 9, images taken at low (2×; Figures 3A-D) and high (20×; Figures 3E-H)) magnification show uniform cellular infiltration into the pores of PUR scaffolds in all scaffold treatment groups with the exception of the upper surface of scaffold nearest the surface which subsequently formed a crust and sloughed away during cleanings associated with dressing changes (Figures 3A-C). At low magnification, the scaffold-treated wounds exhibited infiltration from the lower region of the wound bed and upward filling as evidenced by the intensity gradient in the green staining of newly formed collagen fibrils. Comparison of representative images between Figures 3B and F and Figures 3C and G, respectively, suggested slightly more maturity in collagen formation in the I40 compared to P40 scaffolds. Non-treated wounds were filled with immature granulation tissue consisting of randomly oriented cells and little collagen (Figures 3D and H). The predominant feature in all day 9 wounds was the dense cellularity and relative immaturity compared to later healing periods at days 13 and 30 when increasingly fewer cells were evident and were widely separated by collagen (green) deposition within the extracellular matrix.

By day 13, collagen abundance was increased in all treatment groups as evidenced by less red (cellular component) and more green (collagen component) staining (Figures 3I-L). Cellular density was still dramatically higher in the non-treated wound group compared to all three scaffold-treated wound groups. Cells in non-treated (NT) wounds showed a

distinctly horizontal linearity in their organization (Figure 3L) compared to the wound voids filled with either the injected or preformed scaffold (Figures 3I, J, and K). The persistence of the scaffold appeared to impede linear scar formation and favored a more irregular array of cells. The persistence of the scaffold disrupted the development of parallel alignment of fibrous connective tissue, a process that contributes to wound contraction. Instead, all three scaffold treatments showed a more irregular array of cells with relatively more collagen intensity compared to the NT wound group. All scaffold treatment groups contained less PUR at day 13 than at day 9. Remnants of the scaffold were encircled by a coalescence of macrophages into giant cells that are associated with scaffold degradation[15].

By day 30, the amount of residual scaffold (measured by the percentage of area occupied by PUR in the histological sections) was substantially reduced in I40 and P40 scaffolds compared to earlier time points (Figures 3M and N; Figure 4D) but was not statistically different. Furthermore, collagen accumulation had increased in both I40 and P40 scaffolds as well as the NT group (Figures 3M, N, and O). Three salient differences were observed in the scaffold treatment groups when compared with the non-treated wounds at this time point. The PUR scaffolds were almost entirely degraded into sparsely distributed small particles. Non-treated wounds still showed a horizontal linearity in the array of cells and collagen fiber orientation. The scaffold-treated wounds showed a dramatic reduction in cellular density. The organizational features of the extracellular matrix in the scaffold-treated wounds more closely resembled the original features of the dermis, a dense irregular connective tissue.

Wound contraction was selected as a primary clinical outcome, and was based on photographic images of diminishing surface area over time. All three scaffolds showed significant stenting as compared to non-treated wounds by 2-way ANOVA. When individual groups were compared at each time point, I40 and P40 scaffolds showed significantly less contraction (ie. more stenting) compared to non-treated wounds at day 9 (Figure 4A). At day 30, all scaffolds were almost completely degraded (Figure 4D), yet the stenting effect continued to persist for P40 scaffolds ($p<0.05$; Figure 4A). At the histological level, wound cross-sectional area decreased with time for all wound treatment groups (Figure 4B). At day 30, P40 scaffolds showed a modest but significantly larger wound area than the NT group. While PUR scaffolds delayed undesirable wound contraction at early and intermediate time points (up to day 13), at longer time points the degraded scaffolds showed diminished capacity to effectively stent the wounds at longer time points.

Epithelialization (resurfacing) and scaffold degradation profiles were evaluated using trichrome-stained sections. Resurfacing from the wound edges in these full thickness wounds at day 9 was not significantly different between treatment groups although P40 scaffolds lagged slightly behind the other treatment groups. The accelerated resurfacing effect in non-treated wounds may be a secondary feature attributable to the enhanced wound contraction in NT wounds compared to P40 scaffolds. Wounds treated with P40 scaffolds continued to show less extensive epithelialization (resurfacing) than non-treated wounds at day 13 (Figure 4C). By day 30, epithelialization had equalized among all groups. There were no obvious deleterious effects of the material or the presence of the scaffold on the important process of wound resurfacing over time.

The progression of scaffold degradation was evaluated by measuring the fractional area of PUR remaining within the wound (Figure 4D). At 9 days, I70-treated scaffolds showed less residual PUR compared to I40 and P40 groups, which is consistent with the fact that the I70 scaffolds initially contained less polymer (Table 2). At day 13, P40 scaffolds showed significantly more residual polymer than both the I70 and I40 groups. However, by day 30, the residual percentage of area occupied by PUR in both I40 and P40 scaffolds was not significantly different.

The histological evidence from trichrome-stained sections (Fig. 3) and the quantitative evidence in Figures 4A-D suggest that PUR scaffolds changed the dynamics of wound contraction. We sought another confirmatory method to quantify the effects of delayed contraction on wound healing. Figure 5 shows both quantitative (Figure 5A) and qualitative (Figures 5B-D) data illustrating alignment of collagen fibrils for each of the treatment groups. At 13 days, directional variance values indicated significantly more disordered fiber alignment in the I40 and P40-treated wounds compared to the NT and I70 wounds ($p < 0.05$). Figure 5B shows a representative pseudocolored image of a trichome-stained section of a non-treated wound exhibiting a lower degree of random orientation (lack of variance resulting from a linear alignment of collagen fibers) in a trichrome-stained section of NT wounds. Both non-treated and I70-treated wounds exhibited substantial wound scarring and contraction (Figure 4A). Pseudocolor representation of alignment in I40- and P40-treated wounds showed a higher degree of random orientation (red) in conjunction with persistent remnants of scaffold (Figures 5C-D). Disordered arrangement of collagen fibers (higher angles of orientation) was not significant at either Day 9 or Day 30 (data not shown). The significant, transient disruption in the typical alignment of collagen fibers at day 13 in both I40 and P40 scaffolds (Figure 5A) suggests that PUR scaffolds may help to mitigate scar formation.

Scaffold Impact on Cell Proliferation and Apoptosis

At day 9, wounds treated with all 3 types of scaffolds had significantly more $Ki67^{+}$ (proliferating) cells than non-treated wounds (Figure 6A). Between days 9 and 13, the number of proliferating cells diminished in all treatment groups. By day 13, no significant differences were observed between any of the treatment groups (Figure 6A). These data show that PUR scaffolds provide a favorable environment that supports initial cell proliferation. The diminished proliferative level in the non-treated wound group at day 9 provides evidence that voids filled with scaffolds exhibit a different wound healing dynamic that is indicative of a delay in maturation of the granulation tissue. Apoptosis was evaluated using TUNEL staining (Figure 6B). I40 and P40 scaffolds showed significantly higher apoptotic cells than non-treated wounds at day 9. By day 13, this difference compared to non-treated wounds was only apparent in wounds treated with P40 scaffolds (Figure 6B).

Scaffold Impact on Macrophage Presence

The abundance of macrophages in the tissue was quantified from sections that were immunostained with the MAC387 antibody (Figure 6C). Macrophage numbers were significantly different among the four treatment groups ($p<0.001$). On day 9, wounds treated with I70 scaffolds showed a remarkable influx of macrophages compared to other wounds (p

<0.05). In addition, wounds treated with P40 scaffolds had five times as many MAC387$^+$ cells as non-treated wounds ($p < 0.05$). Macrophage presence declined from day 9 to day 13 in all treatment groups. These data provide evidence that PUR scaffolds do not evoke or prolong a deleterious inflammatory response. Macrophage numbers were negligible or non-detectable in all wounds at the day 30 time point (data not shown).

Scaffold Impact on Blood Vessel Formation

Factor VIII immunostaining was used to assess blood vessel formation in the granulation tissue at days 9 and 13 (Figure 6D). This parameter of wound healing did not show remarkable differences among the four treatment groups at day 9, but did show significance at day 13 among the four groups. Unlike the other parameters (i.e., cell proliferation, cellular apoptosis, and macrophage influx), capillary density (as measured by percentage of area occupied by blood vessels) was sustained at both 9 and 13 days.

Discussion

In this study, we evaluated the suitability of injected polyurethane (PUR) scaffolds to mitigate wound contraction and thereby improve wound healing in a porcine excisional model. We have previously reported that preformed PUR scaffolds are compatible with the processes of wound repair in both the rat [13] and porcine excisional models [24]. However, preformed scaffolds have limitations as void fillers when wound beds have an uneven topography, as is frequently the case in large traumatic tissue deficits or in various chronic wound types. The present study examined whether the favorable properties of preformed PUR scaffolds could be replicated with a flowable, injected formulation that would not need trimming at the time of application, would conform to the dimensions of the wound bed, and could be cured in a moist environment. Our data suggest that injected PUR scaffolds behaved similarly to preformed scaffolds.

Previous studies on the use of void-filling scaffolds in porcine excisional wounds have involved implants with multiple layers. In one study, a wound dressing comprising an outer elastomeric membrane and an inner gelatin sponge layer incorporating basic fibroblast growth factor-loaded microspheres resulted in faster wound closure, a thicker epidermis, and better collagen organization than Vaseline-impregnated gauze [30]. An investigation on the use of biodegradable PUR foams sealed with a microporous PUR membrane found that these bilayer scaffolds exhibited no signs of infection and reduced contraction compared to Integra® after 28 days [31,32]. To our knowledge, the use of injectable and settable void-filling scaffolds in porcine cutaneous wounds has not been previously reported. Previous research by our group using injected PUR scaffolds in rat excisional wounds [13] and preformed PUR scaffolds in porcine excisional wounds [24] has shown that PUR scaffolds are biocompatible, stent wounds to reduce wound contraction, and support cellular infiltration. The present study provides further evidence that both preformed and injected PUR scaffolds facilitate wound healing, support tissue infiltration and matrix production, delay or reduce wound contraction, and reduce scarring in a clinically relevant animal model.

Injected formulations of the PUR scaffolds were characterized *in vitro* to ensure that they had the appropriate characteristics to proceed forward to *in vivo* examination. PUR scaffolds

had working and setting times of 4.8 ± 1.2 min and 16 ± 3 min, respectively, a period of time that is rapid enough to be feasible and appropriate for application in the clinical setting [12]. To assess the inter-connectivity of the pores, the air permeability of the scaffolds was measured. The permeability of the P40 scaffold after leaching (which approximates the *in vivo* conditions after injection and setting) was $1.4 \pm 0.1 \times 10^{-9}$ m^2, which is slightly less than that of conventional open-cell poly(ester urethane) foams [33]. Removal of the low-porosity film on the surface doubled the permeability of the foam ($2.9 \pm 0.6 \times 10^{-9}$ m^2), which indicates that the ~50 μm thick film at the surface has a significant effect on air permeability. Interestingly, the permeability of the P40 scaffolds was two orders of magnitude larger than that of gas-blown PUR scaffolds with 15% carboxymethylcellulose (CMC), while the porosity was about 13% lower [24]. Thus, increasing the porogen from 15% to 40% resulted in a substantial increase in pore connectivity, considering the 100-fold increase in permeability, and a modest decrease in porosity with increasing porogen concentration.

In the porcine excisional wound study, the number of proliferating cells and blood vessel density decreased from day 9 to day 13 in I40, P40, and NT groups (Figure 6). Moreover, images of trichrome staining provide evidence that collagen accumulation increased from day 9 to day 13 in all treatment groups. These results suggest that the wounds were progressing from the proliferative phase of healing to the remodeling phase by day 13.

Our findings show that the injectable PUR scaffold needs further optimization. Both I40 and P40 scaffolds stented the wounds at 9 and 13 days, thereby delaying unwanted wound contraction compared to non-treated and I70-treated wounds (Figure 4A). At day 13, both I40 and P40 scaffolds showed less alignment of cells and collagen fibers than I70 scaffolds and non-treated wounds, which is indicative of less scarring. Hence, the stenting effect (minimalization of wound contraction) is a favorable property. The enhanced healing observed for I40 and P40 scaffolds at intermediate time points is attributed to the mechanical and degradation properties of the scaffolds. The initial bulk modulus of the P40 scaffold after leaching was 50 ± 20 kPa, which is comparable to the 35 kPa reported for the bulk modulus of dermal tissue [34]. Thus, at early time points when degradation of the scaffold was incomplete, the I40 and P40 scaffolds stented the wounds and hindered contraction. While the initial bulk modulus of scaffolds incorporating 70% sucrose was comparable to those with 40% sucrose, the I70 scaffolds degraded significantly faster than P40 scaffolds (Figure 4D). Consequently, I70 scaffolds did not delay contraction or reduce scarring compared to non-treated wounds and this version of the injectable scaffold was eliminated from further investigation The primary limitations of the current formulations appeared at the 30 day timepoint, at which time the I70, I40, and P40 scaffolds had almost completely degraded. As a result, there were no significant differences in residual PUR, wound area, wound contraction, or scarring values among any of the treatment groups. These observations are consistent with a recent study reporting that the scaffold should persist in the wound throughout the remodeling phase (up to 30 days in pigs) in order to minimize scar formation [35]. Further refinement of scaffold persistence and stenting will be necessary to establish that an injectable PUR scaffold will be capable of eliminating wound contracture in the late stages of healing. Our future work will focus on development of scaffolds with slower degradation rates to test the hypothesis that injectable PUR scaffolds can

substantially mitigate or eliminate wound contracture and restore the skin to its former aesthetic and functional properties.

In all scaffold-treated groups, the amount of residual polymer decreased over time with few fragments remaining by day 30 (Figure 4D). Furthermore, the number of MAC387$^+$ macrophages was elevated in scaffold-treated wounds compared to non-treated wounds at day 9. These observations are consistent with the mechanism of oxidative degradation of lysine-derived PUR scaffolds as mediated by macrophages [18]. In non-treated wounds, macrophage numbers decreased between days 9 and 13, which is consistent with previous reports that macrophage numbers usually peak four to five days after wounding [36]. Similarly, in the scaffold-treated groups the number of MAC387$^+$ macrophages decreased significantly from day 9 to 13 (Figure 6C) as the percentage in area of the residual polymer decreased (Figure 6D), which suggests that the elevated inflammatory response on day 9 is transient and associated with the presence of the scaffold [12]. We have recently designed poly(thioketal urethane) (PTKUR) scaffolds from hexamethylene diisocyanate trimer (HDIt) and poly(thioketal) (PTK) diols that undergo first-order oxidative degradation *in vitro* and *in vivo* [37]. In contrast to the LTI-based poly(ester urethane) scaffolds used in this study that exhibited significant degradation during the remodeling phase (Figure 4D), HDIt-based PTKUR scaffolds lost only 40% of their initial mass at seven weeks when implanted in rat excisional wounds. Thus, further optimization of the PUR scaffolds (in either injected or preformed formulations) is anticipated to improve stenting of the wound by tuning the bulk modulus of the scaffold to that of host dermal tissue and extending the persistence of the scaffold throughout the remodeling phase of the healing process.

Conclusions

Injectable and settable PUR scaffolds with high permeability, dermis-like bulk modulus, and working and setting times appropriate for the clinical setting supported ingrowth of new tissue and degraded while facilitating repair in full-thickness porcine excisional wounds. Scaffolds exhibited a moderate stenting effect that delayed wound contraction and reduced scarring at 13 days. Cell proliferation and blood vessel formation were similar in all treatment groups, while macrophage numbers were slightly elevated in scaffold-treated wounds since the PUR scaffolds degraded in response to reactive oxygen species secreted by macrophages. These findings suggest that PUR scaffolds support tissue infiltration and wound healing in a porcine excisional wound model and that applying PUR scaffolds by injection rather than implantation does not adversely affect the wound healing process or scaffold biodegradation.

Acknowledgments

Research reported in this publication was supported by the National Institute of Arthritis and Musculoskeletal and Skin Diseases of the National Institutes of Health under Award Number AR056138, by Kinetic Concepts, Inc (KCI), an Acelity company and by the Department of Veterans Affairs. The content is solely the responsibility of the authors and does not necessarily represent the official views of the National Institutes of Health.

References

1. Sen CK, Gordillo GM, Roy S, Kirsner R, Lambert L, Hunt TK, Gottrup F, Gurtner GC, Longaker MT. Human skin wounds: a major and snowballing threat to public health and the economy. Wound Repair Regen. 2009; 17(6):763–71. [PubMed: 19903300]
2. Zhao G, Usui ML, Lippman SI, James GA, Stewart PS, Fleckman P, Olerud JE. Biofilms and Inflammation in Chronic Wounds. Adv Wound Care (New Rochelle). 2013; 2(7):389–399. [PubMed: 24527355]
3. Volk SW, Iqbal SA, Bayat A. Interactions of the Extracellular Matrix and Progenitor Cells in Cutaneous Wound Healing. Adv Wound Care (New Rochelle). 2013; 2(6):261–272. [PubMed: 24527348]
4. Clark RAF, Ghosh K, Tonnesen MG. Tissue engineering for cutaneous wounds. Journal of Investigative Dermatology. 2007; 127(5):1018–1029. [PubMed: 17435787]
5. Mikos AG, Kretlow JD, Klouda L. Injectable matrices and scaffolds for drug delivery in tissue engineering. Adv Drug Deliv Rev. 2007; 59(4-5):263–273. [PubMed: 17507111]
6. Belkoff SM, Deramond H, Wright NT. Temperature elevation caused by bone cement polymerization during vertebroplasty. Bone. 1999; 25(2):17s–21s. [PubMed: 10458268]
7. Laurencin CT, Khan Y, Yaszemski MJ, Mikos AG. Tissue engineering of bone: Material and matrix considerations. Journal of Bone and Joint Surgery-American Volume. 2008; 90A:36–42.
8. Eccleston GM, Boateng JS, Matthews KH, Stevens HNE. Wound healing dressings and drug delivery systems: A review. Journal of Pharmaceutical Sciences. 2008; 97(8):2892–2923. [PubMed: 17963217]
9. Mostow EN, Haraway GD, Dalsing M, Hodde JP, King D. Grp OVUS. Effectiveness of an extracellular matrix graft (OASIS Wound Matrix) in the treatment of chronic leg ulcers: A randomized clinical trial. Journal of Vascular Surgery. 2005; 41(5):837–843. [PubMed: 15886669]
10. Cheng J, SW P, MM H. Collagen and injected fillers. Otolaryngol Clin North Am. 2002; 35:73–83. [PubMed: 11781208]
11. Baumann L, Kaufman J, Saghari S. Collagen fillers. Dermatol Ther. 2006; 19(3):134–40. [PubMed: 16784512]
12. Adolph EJ, Hafeman AE, Davidson JM, Nanney LB, Guelcher SA. Injectable polyurethane composite scaffolds delay wound contraction and support cellular infiltration and remodeling in rat excisional wounds. J Biomed Mater Res A. 2012; 100A:450–461. [PubMed: 22105887]
13. Adolph EJ, Hafeman AE, Davidson JM, Nanney LB, Guelcher SA. Injectable Polyurethane Composite Scaffolds Delay Wound Contraction and Support Cellular Infiltration and Remodeling in Rat Excisional Wounds. Wound Repair and Regeneration. 2011; 19(2):A9–A9.
14. Hafeman A, Li B, Yoshii T, Zienkiewicz K, Davidson J, Guelcher S. Injectable biodegradable polyurethane scaffolds with release of platelet-derived growth factor for tissue repair and regeneration. Pharm Res. 2008; 25(10):2387–99. [PubMed: 18516665]
15. Hafeman AE, Zienkiewicz KJ, Zachman AL, Sung HJ, Nanney LB, Davidson JM, Guelcher SA. Characterization of the degradation mechanisms of lysine-derived aliphatic poly(ester urethane) scaffolds. Biomaterials. 2011; 32(2):419–29. [PubMed: 20864156]
16. Nelson CE, Gupta MK, Adolph EJ, Shannon JM, Guelcher SA, Duvall CL. Sustained local delivery of siRNA from an injectable scaffold. Biomaterials. 2012; 33(4):1154–61. [PubMed: 22061489]
17. Nelson CE, Kim AJ, Adolph EJ, Gupta MK, Yu F, Hocking KM, Davidson JM, Guelcher SA, Duvall CL. Tunable delivery of siRNA from a biodegradable scaffold to promote angiogenesis in vivo. Adv Mater. 2014; 26(4):607–14, 506. [PubMed: 24338842]
18. Guelcher SA, Hafeman AE, Zienkiewicz KJ, Zachman AL, Sung HJ, Nanney LB, Davidson JM. Characterization of the degradation mechanisms of lysine-derived aliphatic poly(ester urethane) scaffolds. Biomaterials. 2011; 32(2):419–429. [PubMed: 20864156]
19. Dumas JE, Zienkiewicz K, Tanner SA, Prieto EM, Bhattacharyya S, Guelcher S. Synthesis and Characterization of an Injectable Allograft Bone/polymer Composite Bone Void Filler with Tunable Mechanical Properties. Tissue Eng Part A. 2010; 16(8):2505–18. [PubMed: 20218874]

20. Adhikari R, Gunatillake PA, Griffiths I, Tatai L, Wickramaratna M, Houshyar S, Moore T, Mayadunne RT, Field J, McGee M, et al. Biodegradable injectable polyurethanes: synthesis and evaluation for orthopaedic applications. Biomaterials. 2008; 29(28):3762–70. [PubMed: 18632149]
21. Guelcher SA, Li B, Davidson JM. The effect of the local delivery of platelet-derived growth factor from reactive two-component polyurethane scaffolds on the healing in rat skin excisional wounds. Biomaterials. 2009; 30(20):3486–3494. [PubMed: 19328544]
22. Guelcher SA, Li B, Brown KV, Wenke JC. Sustained release of vancomycin from polyurethane scaffolds inhibits infection of bone wounds in a rat femoral segmental defect model. Journal of Controlled Release. 2010; 145(3):221–230. [PubMed: 20382191]
23. Sullivan TP, Eaglstein WH, Davis SC, Mertz P. The pig as a model for human wound healing. Wound Repair Regen. 2001; 9(2):66–76. [PubMed: 11350644]
24. Adolph EJ, Pollins AC, Cardwell NL, Davidson JM, Guelcher SA, Nanney LB. Biodegradable lysine-derived polyurethane scaffolds promote healing in a porcine full-thickness excisional wound model. J Biomater Sci Polym Ed. 2014; 25(17):1973–85. [PubMed: 25290884]
25. Guelcher S, Srinivasan A, Hafeman A, Gallagher K, Doctor J, Khetan S, McBride S, Hollinger J. Synthesis, In vitro degradation, and mechanical properties of two-component poly(ester urethane)urea scaffolds: Effects of water and polyol composition. Tissue Engineering. 2007; 13(9): 2321–2333. [PubMed: 17658992]
26. Nanney LB, Woodrell CD, Greives MR, Cardwell NL, Pollins AC, Bancroft TA, Chesser A, Michalak M, Rahman M, Siebert JW, et al. Calreticulin enhances porcine wound repair by diverse biological effects. Am J Pathol. 2008; 173(3):610–30. [PubMed: 18753412]
27. Okwueze MI, Cardwell NL, Pollins AC, Nanney LB. Modulation of porcine wound repair with a transfected ErbB3 gene and relevant EGF-like ligands. J Invest Dermatol. 2007; 127(5):1030–41. [PubMed: 17124505]
28. Fonck E, Feigl GG, Fasel J, Sage D, Unser M, Rufenacht DA, Stergiopulos N. Effect of aging on elastin functionality in human cerebral arteries. Stroke. 2009; 40(7):2552–6. [PubMed: 19478233]
29. Rezakhaniha R, Agianniotis A, Schrauwen JT, Griffa A, Sage D, Bouten CV, van de Vosse FN, Unser M, Stergiopulos N. Experimental investigation of collagen waviness and orientation in the arterial adventitia using confocal laser scanning microscopy. Biomech Model Mechanobiol. 2012; 11(3-4):461–73. [PubMed: 21744269]
30. Huang S, Deng T, Wu H, Chen F, Jin Y. Wound dressings containing bFGF-impregnated microspheres. Journal of Microencapsulation. 2006; 23(3):277–290. [PubMed: 16801240]
31. Greenwood JE, Dearman BL. Split skin graft application over an integrating, biodegradable temporizing polymer matrix: immediate and delayed. J Burn Care Res. 2012; 33(1):7–19. [PubMed: 22079917]
32. Greenwood JE, Dearman BL. Comparison of a sealed, polymer foam biodegradable temporizing matrix against Integra(R) dermal regeneration template in a porcine wound model. J Burn Care Res. 2012; 33(1):163–73. [PubMed: 22002205]
33. Dawson MA, Germaine JT, Gibson LJ. Permeability of open-cell foams under compressive strain. Int J Solids and Structures. 2007; 44(16):5133–45.
34. Pailler-Matteia C, Beca S, Zahouani Z. In vivo measurements of the elastic mechanical properties of human skin by indentation tests. Medical Eng and Physics. 2008; 30:599–606.
35. Lorden ER, Miller KJ, Bashirov L, Ibrahim MM, Hammett E, Jung Y, Medina MA, Rastegarpour A, Selim MA, Leong KW, et al. Mitigation of hypertrophic scar contraction via an elastomeric biodegradable scaffold. Biomaterials. 2015; 43:61–70. [PubMed: 25591962]
36. Braiman-Wiksman L, Solomonik I, Spira R, Tennenbaum T. Novel insights into wound healing sequence of events. Toxicol Pathol. 2007; 35(6):767–79. [PubMed: 17943650]
37. Martin JR, Gupta MK, Page JM, Yu F, Davidson JM, Guelcher SA, Duvall CL. A porous tissue engineering scaffold selectively degraded by cell-generated reactive oxygen species. Biomaterials. 2014; 35(12):3766–76. [PubMed: 24491510]

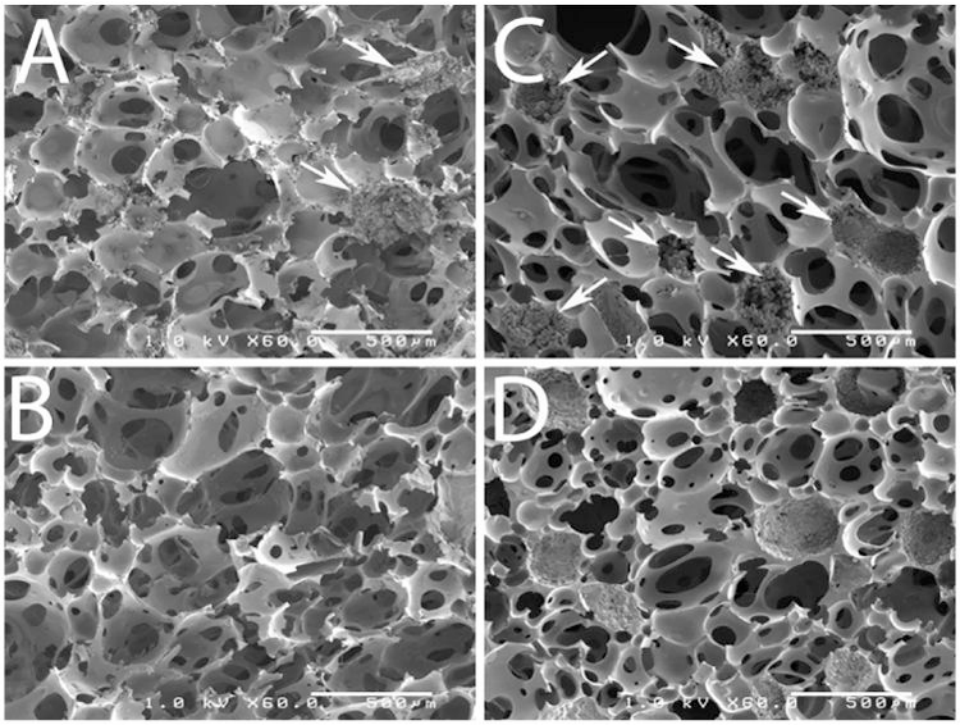

Figure 1.

SEM images of PUR scaffolds. Panels A and B show scaffolds constructed with 40% sucrose before (A) and after (B) leaching. Panels C and D show scaffolds constructed with 70% sucrose before (C) and after (D) leaching. Arrows indicate sucrose beads embedded in pore walls. Scale bar = 500 microns

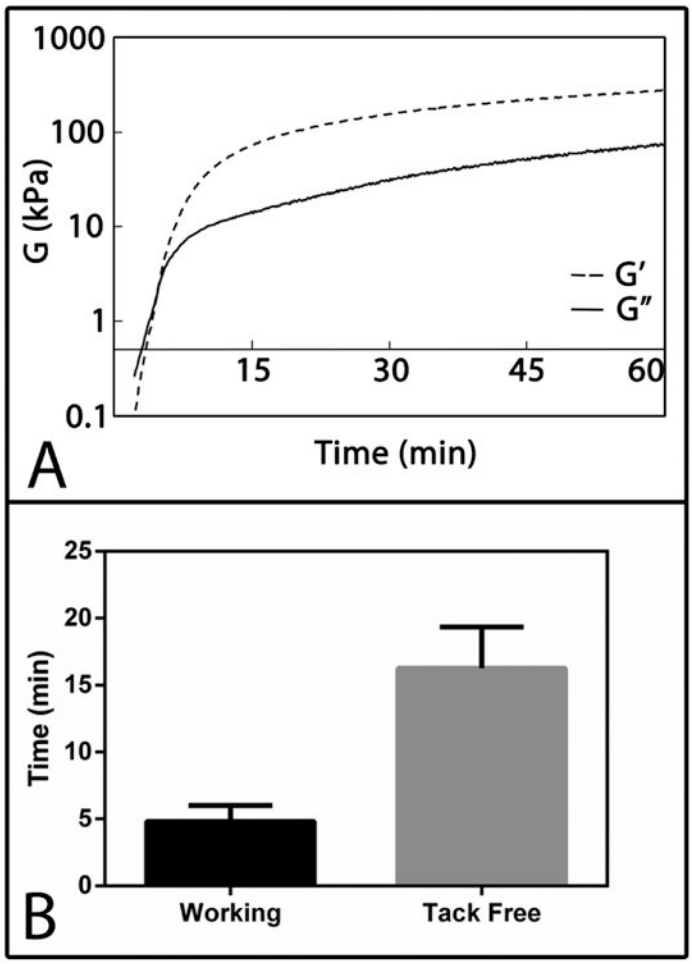

Figure 2.

Rheological properties of PUR scaffolds. (A) Representative cure profile of a scaffold with 40% sucrose. Vertical dashed line indicates G-crossover point, which was used to determine the working time. (B) Mean working and tack-free times of scaffolds with 40% sucrose.

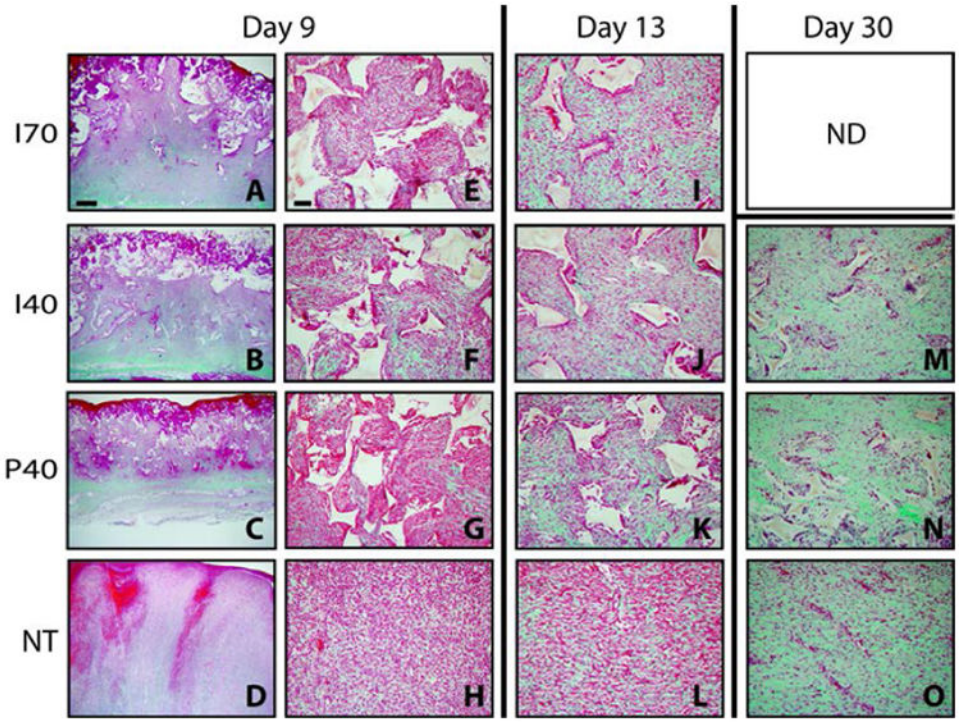

Figure 3.

Representative images of trichrome staining at day 9 with paired magnifications of 2× (left) and 20× (right). Wounds at days 13 and 30 are shown at 20× with the exception of Section M, which shows a day 30 wound injected with a scaffold with 40% sucrose at a 2× magnification. Mature collagen is intense green, nascent collagen is pale green, cytoplasm and fibrin are red or pink. PUR scaffold remnants remain unstained and appear white with angular profiles. Scale bar in A (2× magnification) = 1000 μm; Scale bar in E (20× magnification) = 100 μm.

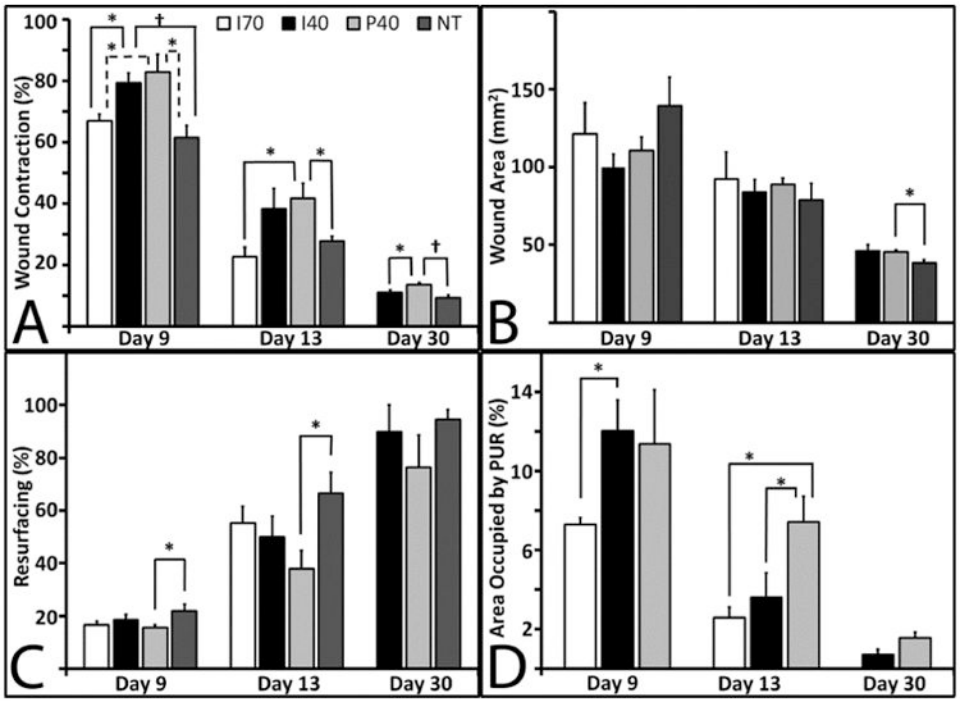

Figure 4. Scaffold effects on porcine full-thickness excisional wound dimensions

For I70 at 9 and 13 days, n=4; For I40, P40, and NT, n=9 at 9 and 13 days, and n=5 at 30 days. Bars represent standard error of the mean. (A) Wound contraction measured from surface images. This graph represents the diminishing surface area as the wounds contract. A two-way ANOVA was performed to compare differences between the three time points and three treatment groups and the test of significance was met ($p \leq 0.05$). Day 9 (solid bars) and day 13 wounds (light grey bars) showed significance among the groups ($p < 0.05$). At day 30 (dark grey), significance was noted among the groups ($p < 0.05$). (B) Cross-sectional area of wounds. At day 30, P40 wounds were significantly larger than NT wounds ($p < 0.05$). (C) Percent resurfacing. Resurfacing of P40 scaffolds was significantly lower than that of non-treated wounds at days 9 and 13. (D) Percent of residual PUR in the wound was significantly different at Day 13 ($p = 0.05$) by ANOVA among the 3 different groups. At day 13, P40 levels were significantly higher than both I70 and I40 treatments ($p < 0.05$).

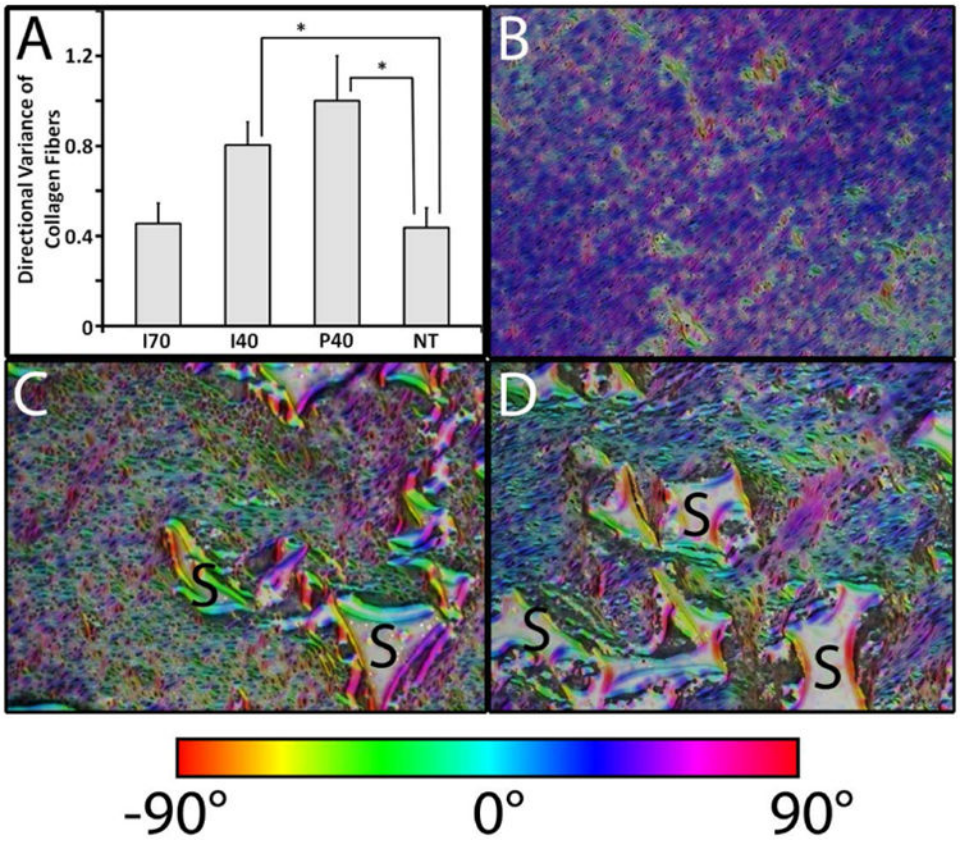

Figure 5.

Scaffold effects on the orientation of collagen fibers and cells in porcine full-thickness excisional wounds at Day 13. (A) Directional variance of alignment calculated from low-magnification images (2×) of histological sections. Significant differences (*, $p < 0.05$) were found between either I40 or P40 and NT treatment groups. (B-D) Representative images of Orientation J (ImageJ plug-in) generated HSB color-coded maps visualizing fiber orientation for NT (B), I40 (C), and P40 (D). Residual PUR was labeled with “S”.

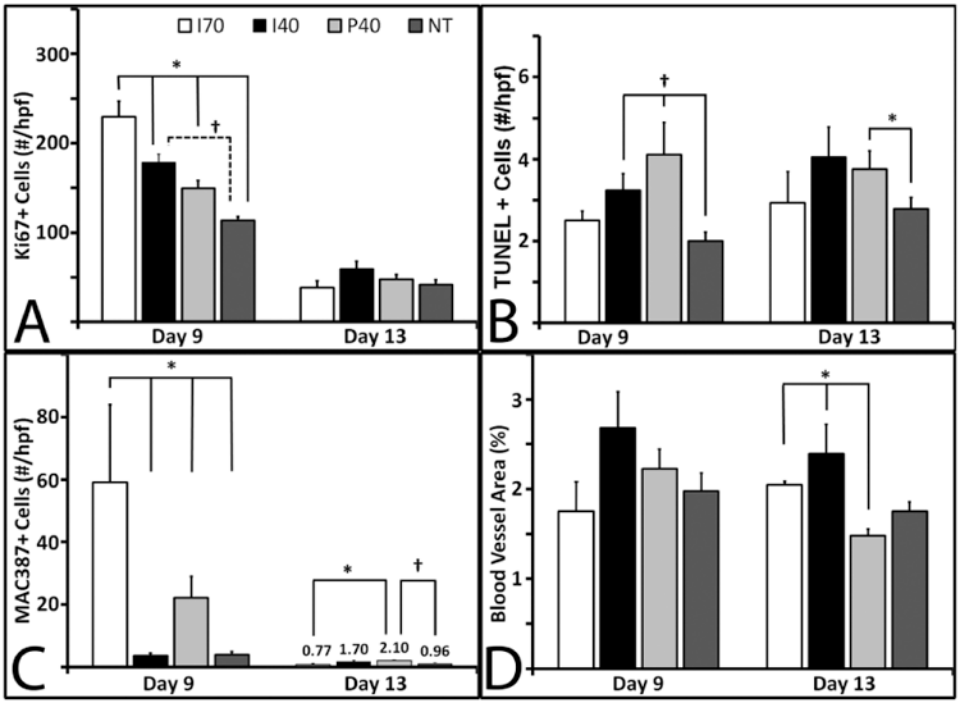

Figure 6.

Immunohistochemical measurements. Unless noted, for day 9 samples, I70, n=3; I40 and P40, n=8; and NT, n=9. For Day 13, I70, n=3; I40, n=7; and P40 and NT, n=9. Bars represent standard error of the mean. (A) Quantification of $Ki67^+$ immunostaining at days 9 (solid bars) and 13 (grey bars). A significant difference ($p \leq 0.001$) was observed among all groups at day 9. NT at day 9, n=8. (B) Quantification of $TUNEL^+$ immunostaining at days 9 and 13. At day 9 the difference between the I40, P40, and NT groups was significant ($p<0.05$). (C) Quantification of $MAC387^+$ immunostaining among the groups at days 9 and 13. Macrophage presence was significant at day 9 ($p<0.001$). (D) Quantification of $TUNEL^+$ staining at days 9 and 13 only showed significance by ANOVA at Day 13 ($p<0.001$).

Table 1

In vivo study design (5 Yorkshire pigs).

		# of replicates at each time point (n)		
Treatment Group	**Name**	**9 days**	**13 days**	**30 days**
Not Treated, Empty defect (negative control)	NT	9	9	5
Preformed Scaffold + 40% sucrose	P40	9	9	5
Injected Scaffold + 40% sucrose	I40	9	9	5
Injected Scaffold + 70% sucrose	I70	4	4	0

Table 2

Physical and mechanical properties of PUR scaffolds formulated with 40% or 70% sucrose before and after leaching. Data are expressed as mean ± standard deviation.

	Scaffold with 40% Sucrose		Scaffold with 70% Sucrose	
Leaching	–	+	–	+
Density (kg m^{-3})	490 ± 30	280 ± 20 *	660 ± 60	190 ± 10 *
Porosity (%)	59 ± 3	77 ± 2 *	45 ± 5	84 ± 1 *
Pore Size (μ)	280 ± 80	290 ± 110	300 ± 140	250 ± 80
Bulk Modulus (kPa)	70 ± 40	50 ± 20	150 ± 30	50 ± 10 *

Asterisks indicate significant difference before and after leaching ($p < 0.01$).

Table 3

Permeability of PUR scaffolds containing 40% or 70% sucrose foamed in dry or wet environments with (+) or without (-) the surface film. Leaching of the scaffolds significantly increased their permeability ($p < 0.01$).

Sample	Sucrose	Leaching	Environment	Film	Permeability (10^{-10} m^2)	Significance
A	70%	–	Dry	+	4.1 ± 1.8	†
B	70%	+	Dry	+	7.3 ± 1.6	‡
C	70%	–	Wet	+	9.4 ± 1.9	‡
D	70%	+	Wet	+	19.6 ± 3.2	
E	40%	–	Dry	+	1.5 ± 0.2	*
F	40%	+	Dry	+	1.7 ± 0.1	*
G	40%	–	Wet	+	4.4 ± 0.5	†
H	40%	+	Wet	+	14.2 ± 0.6	
I	40%	–	Dry	–	3.3 ± 1.5	*
J	40%	+	Dry	–	7.7 ± 2.2	‡
K	40%	–	Wet	–	19.0 ± 6.2	
L	40%	+	Wet	–	28.9 ± 6.1	

Asterisks indicate significant difference from samples D, K, and L ($p < 0.05$).

Daggers indicate significant difference from samples D and L ($p < 0.05$).

Double dagger indicates significant difference from sample L ($p < 0.05$).